International Journal of
Environmental Research and Public Health

MDPI

Article

Impact of Different Lignin Sources on Nitrogen−Doped Porous Carbon toward the Electrocatalytic Oxygen Reduction Reaction

Zheng Li [1], Yuwei Feng [1], Xia Qu [1], Yantao Yang [1,2], Lili Dong [1,2], Tingzhou Lei [1,2] and Suxia Ren [1,2,*]

[1] Institute of Urban & Rural Mining, Changzhou University, Changzhou 213164, China
[2] Changzhou Key Laboratory of Biomass Green, Safe & High Value Utilization Technology, Changzhou 213164, China
* Correspondence: rensuxia@cczu.edu.cn

Abstract: Lignin is an ideal carbon source material, and lignin−based carbon materials have been widely used in electrochemical energy storage, catalysis, and other fields. To investigate the effects of different lignin sources on the performance of electrocatalytic oxygen reduction, different lignin−based nitrogen−doped porous carbon catalysts were prepared using enzymolytic lignin (EL), alkaline lignin (AL) and dealkaline lignin (DL) as carbon sources and melamine as a nitrogen source. The surface functional groups and thermal degradation properties of the three lignin samples were characterized, and the specific surface area, pore distribution, crystal structure, defect degree, N content, and configuration of the prepared carbon−based catalysts were also analyzed. The electrocatalytic results showed that the electrocatalytic oxygen reduction performance of the three lignin−based carbon catalysts was different, and the catalytic performance of N−DLC was poor, while the electrocatalytic performance of N−ELC was similar to that of N−ALC, both of which were excellent. The half−wave potential ($E_{1/2}$) of N−ELC was 0.82 V, reaching more than 95% of the catalytic performance of commercial Pt/C ($E_{1/2}$ = 0.86 V) and proving that EL can be used as an excellent carbon−based electrocatalyst material, similar to AL.

Keywords: lignin; carbon material; nitrogen doping; oxygen reduction reaction

check for updates

Citation: Li, Z.; Feng, Y.; Qu, X.; Yang, Y.; Dong, L.; Lei, T.; Ren, S. Impact of Different Lignin Sources on Nitrogen−Doped Porous Carbon toward the Electrocatalytic Oxygen Reduction Reaction. *Int. J. Environ. Res. Public Health* **2023**, *20*, 4383. https://doi.org/10.3390/ijerph20054383

Academic Editors: Bo Zhang and Ye Bian

Received: 15 January 2023
Revised: 27 February 2023
Accepted: 27 February 2023
Published: 1 March 2023

Copyright: © 2023 by the authors. Licensee MDPI, Basel, Switzerland. This article is an open access article distributed under the terms and conditions of the Creative Commons Attribution (CC BY) license (https://creativecommons.org/licenses/by/4.0/).

1. Introduction

To solve the increasingly serious energy crisis and reduce environmental pollution, researchers have focused on developing new energy sources. Among them, fuel cells have attracted much attention due to their advantages, such as rich fuel sources, strong energy conversion ability, low operating temperature, and low environmental pollution [1–3]. The oxygen reduction reaction (ORR) is an important cathode reaction in fuel cells and metal–air batteries [4,5]. However, due to the slow kinetics of the ORR, which restricts the energy conversion, electrocatalysts are needed to accelerate the reaction kinetics. To date, platinum−based catalysts are still the most effective ORR catalysts. However, due to their low reserves, high cost, and poor cycle stability, platinum−based catalysts have difficulty meeting the needs of large−scale applications [6]. Therefore, the search for nonmetallic catalysts with low cost and excellent catalytic performance has become a research hotspot.

Porous carbon materials with good electrical conductivity, stable chemical properties, high specific surface area, and abundant porous structure are widely used in electrochemical catalytic research. Lignin is the second−largest biomass resource, second only to cellulose [7–9]. Lignin is a byproduct of industri processes that mainly include pulp− and papermaking (i.e., alkaline lignin) and biorefining waste residues (i.e., enzymatic lignin); however, most lignin is burned as low−calorific fuel to provide heat energy or directly discharged. Previous research showed that only approximately 2% of lignin could be found for high−value utilization [10,11]. In addition, the carbon content of lignin is up to 60%, which can make it a good precursor for preparing carbon materials. Therefore, the use

of lignin as a precursor to prepare carbon materials has great application potential in the future [12–14], especially in the field of electrocatalysis. For example, Graglia [15] used beech lignin as a raw material to prepare microporous, mesoporous, and macroporous nitrogenous carbon materials through alkaline hydrothermal treatment, aromatic nitrification reaction, and roasting activation. Its $E_{1/2}$ in alkaline medium was 0.85 V, showing ORR electrocatalytic activity comparable to that of the most advanced nonprecious metal catalysts. Zhang [16] prepared nitrogen and sulfur co−doped porous carbon with good electrical conductivity by roasting amine lignin sulfonate at high temperature, showing good ORR electrocatalytic activity. Li [17] first proposed synthesis of an Fe−N−C/FePx/NPSC catalyst with a high specific surface area and rich pore structure through a salt−assisted process using sodium lignosulfonate as a carbon precursor, which promoted the catalyst to expose more active sites, increasing the catalytic activity and stability. The half−wave potential $E_{1/2}$ reached 0.9 V, which was superior to the half−wave potential (0.85 V) measured for commercial Pt/C.

It follows, then, that lignin is an excellent raw material for preparing electrocatalytic oxygen reduction catalysts. However, the sources and molecular structure of lignin are complex and variable, and the yield and repeatability of preparing lignin−based carbon materials are low, impeding the preparation and application of lignin−based carbon materials. Therefore, it is necessary to deeply study the basic chemical structure of lignin, and to develop a simple, green, low−cost, large−scale preparation method for the production of lignin−based carbon materials. In addition, alkaline lignin (AL) is the main byproduct in the process of pulp and papermaking and forest biomass refining, with an annual output of over 50 million tons in China. Enzymatic lignin (EL) is a new type of lignin that is separated from the residue of microbial enzymatic hydrolysis processes. Compared with traditional alkaline lignin and sulfate lignin, enzymatic lignin has a variety of active groups and better reactivity. Nevertheless, most research has focused on the utilization of AL in the field of electrocatalytic oxygen reduction [15,18–21], and little research has investigated the development and exploitation of EL. Whether EL is suitable for the preparation of electrocatalytic carbon materials, and what the differences are between lignins that come from different sources, remains to be verified. Therefore, the purpose of this paper is to identify the effects of specific lignin structures on the preparation of heteroatomic porous carbon's electrocatalytic oxygen reduction performance, based on the differences in the structure and properties of different kinds of lignin, to broaden the application field of enzymatic hydrolysis of lignin. In this paper, N−doped porous carbon was prepared with enzymatic hydrolysis lignin (EL), alkaline lignin (AL) and dealkaline lignin (DL) as raw materials and melamine as a nitrogen source to explore the effects of the structural characteristics of different lignin raw materials on its properties.

2. Experimental Materials and Methods

2.1. Experimental Materials

EL was purchased from Shandong Longli Biotechnology Co. Ltd., dealkaline lignin (DL) and melamine ($C_3H_6N_6$, 99%) were purchased from Macklin Chemical Reagent Co., Ltd. (Shanghai, China), AL was purchased from Aladdin Chemical Reagent Co., Ltd. (Shanghai, China), Nafion (Model D520 mass fraction 5%) was purchased from Shanghai Hesen Electric Co., Ltd., and ethanol (analytically pure, 99.7%) was purchased from Jiangsu Qiangsheng Functional Chemical Co., Ltd. (Changshu, China).

2.2. Experimental Procedure

First, 1 g of lignin (EL, AL, and DL) and 4 g of melamine were dispersed in 100 mL of deionized water (90 °C) and stirred for 30 min. Then, 1 g of $ZnCl_2$ was added, heated in a water bath (100 °C), and the mixture was stirred until the deionized water evaporated completely, after which the residue was dried and ground. The sample was placed in a porcelain boat and annealed in a quartz tube. In a N_2 atmosphere, the sample was heated to 900 °C at a rate of 5 °C min^{-1} (the N_2 flow rate was 50~100 mL min^{-1}), held for 2 h,

and then naturally cooled to room temperature. The obtained lignin carbon material was pickled with 1 M hydrochloric acid and then dried to obtain a black lignin carbon material (LC). The mass ratio of lignin, $ZnCl_2$, and melamine was 1:1:4, and the LC samples prepared using enzymatic hydrolysis lignin, alkaline lignin, and dealkaline lignin mixed with $ZnCl_2$ and melamine were labeled N−ELC, N−ALC, and N−DLC, respectively.

2.3. Catalyst Structure Characterization

A Fourier−transform infrared spectrometer (FTIR, Germany, BRUKER−Vertex 70) and UV–Vis absorption spectra (UV−Vis, USA, PE−Lambda 750) were used to determine the types of functional groups in lignin molecules. The contents of different elements (C, H, N, S) in the materials were determined by using the element analyzer (Germany, Elementar−vario MACRO cube). The thermal stability of the materials was tested using an SDT Q600 analyzer (TA Instruments Inc., New Castle, DE, USA). X−ray diffraction (XRD; Germany, Brooker−Bruker D8 ADVANCE) was used to characterize the crystal structure of the materials. The surface composition of the samples was determined by X−ray photoelectron spectroscopy (XPS). Raman spectroscopy, using a Raman microscope, was used to characterize the defect degree of the materials. The morphologies of the carbon materials were characterized by high−resolution transmission electron microscopy (HRTEM) (Japan, JEOL−JEM 2100 F). The specific surface area and pore size distribution were determined by a nitrogen adsorption–desorption test (BET, USA, Mack−ASAP2460).

2.4. Electrocatalytic Performance Test of the Catalyst

The electrochemical tests were conducted using a Shanghai Chenhua CHI760E electrochemical workstation. In this experiment, a three−electrode system was used: the rotating disk electrode (RDE) was the working electrode, the saturated calomel electrode (SCE) was the reference electrode, the platinum plate electrode was the opposite electrode, and the electrolyte solution was 0.1 M KOH. The diameter of the glass carbon electrode of the RDE was 4 mm.

Catalyst samples (2 mg) were dispersed in a 550 μL mixed solution, including 250 μL of ethanol, 250 μL of deionized water, and 50 μL of Nafion solution (5 wt%), and ultrasonicated for 30 min to prepare ink−containing catalysts. The working electrode was prepared by absorbing 12 μL of ink, dropping it on the glass carbon electrode, and drying it naturally at room temperature. A comparison of commercial Pt/C (Johnson Matthey, 20 wt%) catalysts was used to prepare the ink and the working electrodes.

Cyclic voltammetry (CV) and linear sweep voltammetry (LSV) were performed at the working electrodes of the supported catalyst at 0.1 M KOH saturated with O_2 and N_2, respectively. The CV test parameters were in the potential scanning range of 0~1.2 V at a scanning rate of 50 $mV \cdot s^{-1}$. The LSV test parameters were in the potential scanning range of 0~1.2 V at a scanning rate of 5 $mV \cdot s^{-1}$ in an O_2 atmosphere. Without special explanation, the polarization curve at 1600 rpm was selected for comparison in this paper.

3. Results and Discussion

3.1. Analysis of the Basic Properties of Different Lignins

3.1.1. Element Analysis

The preparation process of carbon materials is a process in which carbon elements are rearranged and accompanied by other elements escaping under extreme temperature conditions. Therefore, it is very advantageous to analyze and explore the transformation process of the lignin structure during the preparation of carbon materials by analyzing the elemental composition of lignin molecules. Table 1 shows the elemental compositions of three kinds of lignin: EL, AL, and DL. As shown in Table 1, the C contents of EL, AL, and DL were above 65%, with little difference among them. The C content of AL was the highest (65.74%), while that of EL was lower (65.24%). The high carbon content of lignin proves that it is a valuable carbon source material. In addition, EL, AL, and DL all contain different proportions of trace N and S, which may be related to the different sources of lignin.

Table 1. Chemical characteristics of the nitrogen−doped porous carbons.

Lignin Sources	Element Content (%)			
	C	H	N	S
EL	65.24	5.38	1.05	0.16
AL	65.74	7.30	0.84	0.71
DL	65.45	5.26	0.31	2.56

3.1.2. Molecular Structure Analysis of Different Lignin Species

Figure 1 shows the FTIR spectra of the three different kinds of lignin. It can be seen from the figure that the absorption peaks of the different lignins are effectively the same, indicating the presence of similar functional groups in the molecular structures of several lignins. Several kinds of lignin exhibit strong broad peaks at 3406 cm^{-1}, which can be attributed to the O−H stretching vibration absorption peaks of phenol and alcohol hydroxyl groups in lignin. The weaker absorption peaks at 2938 cm^{-1} and 2840 cm^{-1} represent C−H stretching vibrations in the methyl and methylene functional groups, respectively. The absorption peak in the range of 1602 cm^{-1}~1425 cm^{-1} is caused by the stretching vibration of the aromatic skeleton [22]. The absorption peak at 1120 cm^{-1} is the characteristic absorption of the lilac−based structural unit, which exists in all three lignins. The absorption peak at 1029 cm^{-1} is the C−O bending vibration of secondary alcohol and ether bonds. The characteristic absorption peak at 832 cm^{-1} is the p−hydroxyphenyl (H)−type structural unit. It can be seen from the figure that there are p−hydroxyphenyl structural units in EL and DL, while no characteristic absorption peak of this structural unit can be seen in AL. The absorption peak of EL at 1700 cm^{-1} indicates that it has a more unconjugated carbonyl structure, which indicates that conjugated double bonds in EL are destroyed, and some oxidation or esterification reactions occur [23]. AL and DL exhibit absorption peaks at 620 cm^{-1}, corresponding to aliphatic C−C stretching vibrations, while there is no absorption peak at this position in EL, which proves that EL does not contain this functional group.

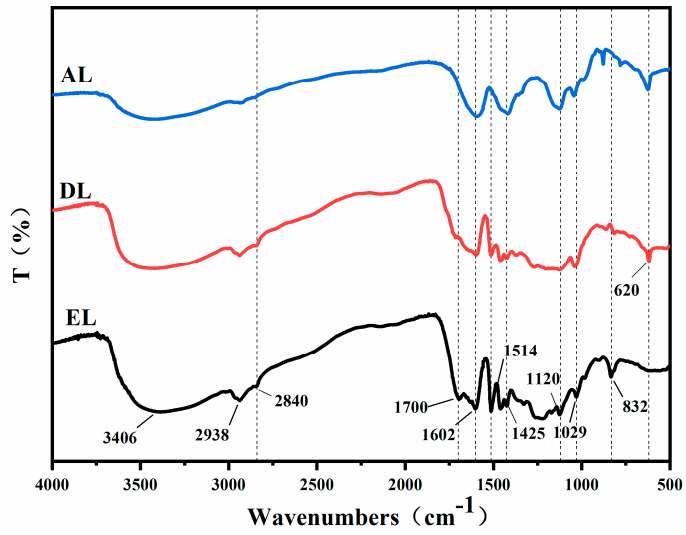

Figure 1. FTIR of different kinds of lignin.

Lignin molecules have ultraviolet absorption groups such as aromatic structures, C=C double bonds, and conjugated C=O groups, which can strongly absorb ultraviolet light. Therefore, ultraviolet absorption spectra can be used to analyze the characteristic peaks of lignin. As shown in Figure 2, EL, DL, and AL all have obvious aromatic ring characteristic absorption peaks at 296 nm, corresponding to the absorption caused by electron transition in conjugated molecular structures, such as aromatic rings. DL and AL

showed wide absorption peaks near 340 nm, corresponding to absorption of coumaric acid and ferulic acid, indicating that these two lignins contained a certain amount of phenolic acid structures. Compared with DL and AL, there was no obvious absorption peak near 340 nm in EL, indicating that there were very few functional groups of phenolic acids in this lignin.

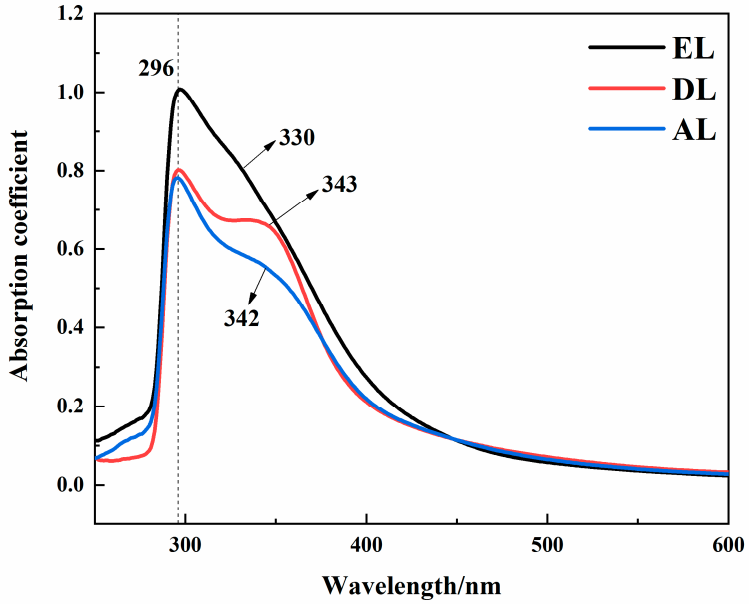

Figure 2. UV−Vis spectra of different kinds of lignin.

Figure 3a,b show the TG and DTG curves of three different kinds of lignin, respectively. According to the figure, the thermal decomposition process of EL can be divided into four stages: the first stage (20~150 °C) is mainly the evaporation of water in lignin, and the sample mass loss rate is 10.4%. The second stage occurs in the temperature range from 150 °C to 240 °C, which is mainly the stage of lignin depolymerization and the temperature range of lignin glass transition, and the sample mass loss rate is 15.8%. In the temperature range from 240 °C to 420 °C, the third stage is the main stage of lignin pyrolysis. During this heating process, lignin undergoes a thermal decomposition reaction, and the branched−chain structure of lignin is largely broken and transformed into a large number of volatile small molecular products (CO, CO_2, H_2O, etc.), with a mass loss rate of 49.4%. The DTG curve shows that the maximum weight loss rate peaks at approximately 333 °C. When the temperature is higher than 420 °C, the chemical bond around the benzene ring breaks, and the benzene ring also breaks and recombines to form aromatic compounds before polymerizing into amorphous carbon. At this time, the thermal decomposition process is essentially completed, which is the fourth stage of pyrolysis [24]. DL and EL have a similar thermal decomposition process, but the mass residual rate of DL is much higher than that of EL because more ash remains after the end of DL pyrolysis. For AL, the pyrolysis process is quite different. AL contains many phenolic hydroxyl groups, most of which are connected with other structural units in the form of ether bonds. The DTG curves show that two maximum values of the thermal decomposition rate appear at 237 °C and 420 °C. This pyrolysis process is mainly manifested as the general breaking of aryl ether bonds and methoxy groups, along with side−chain breaking through dehydration to produce small molecular compounds. The process of lignin carbonization is the rearrangement of carbon atoms at high temperature. Therefore, different thermal cracking processes may affect the structure of the final carbon material and, thus, further affect its electrocatalytic performance.

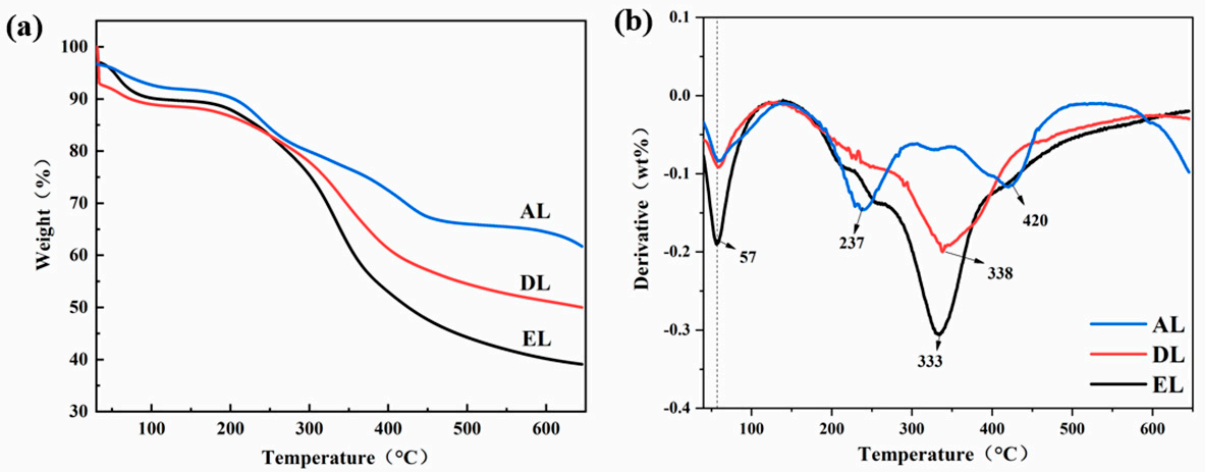

Figure 3. Thermal performance analysis of different kinds of lignin: (**a**) TG curve; (**b**) DTG curve.

3.2. Effect of Catalyst Type and Amount on the Pyrolysis Product Distribution of Nitrogen−Doped Porous Carbons

Figure 4 shows TEM images of different lignin−based carbon materials. As shown in the figure, N−ALC presents the shape of nanoparticles (Figure 4b), while N−ELC and N−DLC show the morphology of carbon nanosheets, which are thin and transparent, showing a graphene−like transparent structure, and folds can be observed (Figure 4a,c). In the high−resolution TEM images (Figure 4d,f), the lattice spacing of the carbon material at approximately 0.34 nm can be clearly seen, which is attributed to the (002) crystal plane of graphitic carbon [19], while the lattice spacing at approximately 0.25 nm in Figure 4e is mainly attributed to the (101) graphitic carbon crystal plane.

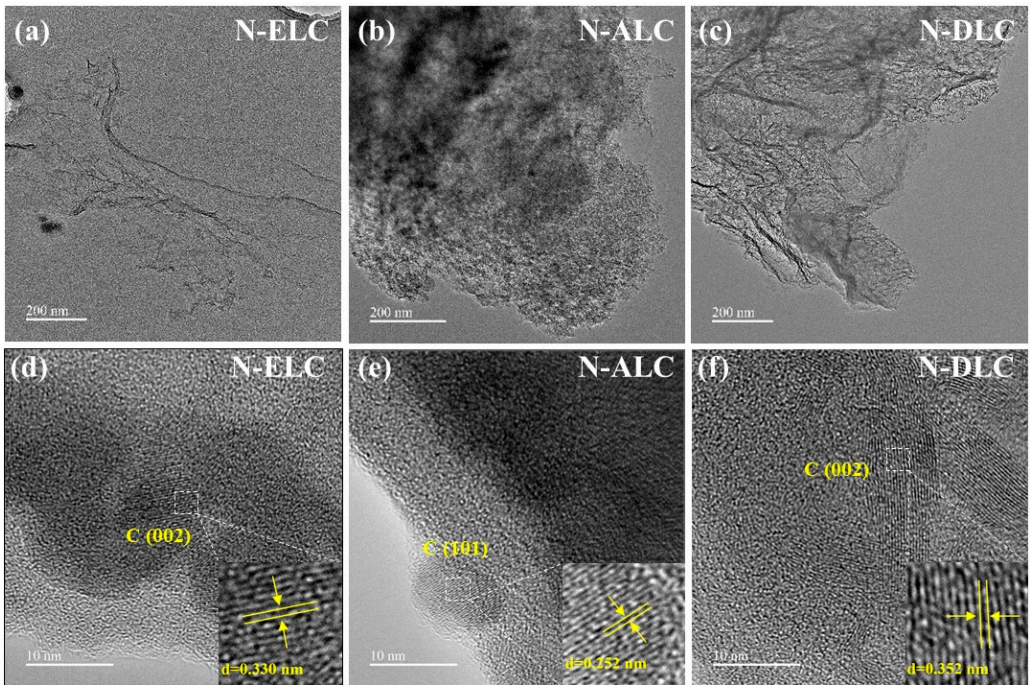

Figure 4. TEM diagrams of different kinds of lignin carbon materials: (**a**,**d**) N−ELC; (**b**,**e**) N−ALC; (**c**,**f**) N−DLC.

It can be seen from the full XPS scan map in Figure 5a that the N 1_S peak is at 398.9 eV. The analysis of N types of porous carbon doped with different lignin−based N is shown in Figure 5b–d. The peaks at binding energies of approximately 397, 398, 399, and 400 eV

correspond to pyridinic nitrogen, pyrrolic nitrogen, graphitic nitrogen, and nitrogen oxide, respectively. Table 2 shows the nitrogen contents and nitrogen types of different samples. It has been proven in many studies that the presence of pyridinic N can improve the onset potential of ORR, while graphitic N can improve the limiting diffusion current density [25]. The highest content of graphitic nitrogen in N−ELC was 43%, and that of pyridinic nitrogen was 25.1%, both of which were higher than those in N−ALC and N−DLC. Therefore, the ORR catalytic performance of N−ELC should theoretically be superior to that of N−ALC and N−DLC. However, the electrocatalytic performance is also affected by the specific surface area and pore volume [26].

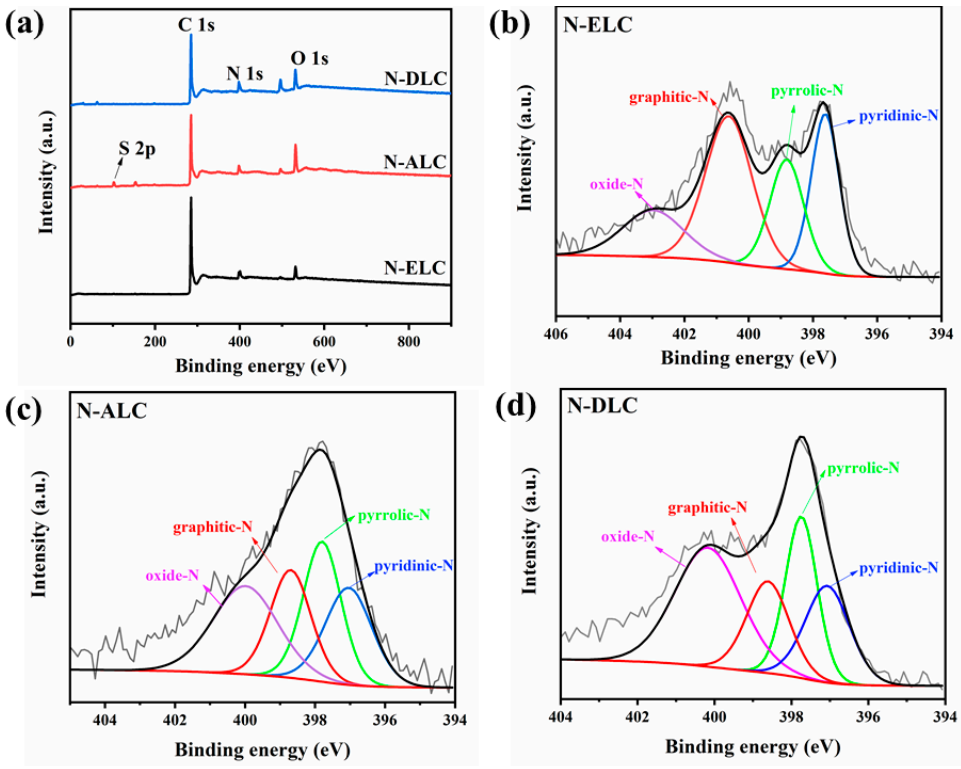

Figure 5. (**a**) XPS full−scan spectra of different lignin carbon materials, and N 1s spectra of (**b**) N−ELC, (**c**) N−ALC, and (**d**) N−DLC.

Table 2. N contents and N types of different lignin materials.

Lignin Carbon Materials	N Content (%)	Percentage of Functional Group Area (%)			
		N Oxide	Graphitic N	Pyrrolic N	Pyridinic N
N−ELC	8.89	12.7	43.0	19.3	25.1
N−ALC	7.33	28.1	22.4	26.3	23.2
N−DLC	11.38	38.0	17.9	24.1	20.0

Raman characterization can be used to further analyze the changes in the defect degree of the carbon material structure. As shown in Figure 6a, the D band (1350 cm^{-1}) and G band (1580 cm^{-1}) represent the lattice defects of carbon atoms and the stretching vibration of the sp^2 hybrid orbital plane of the carbon atoms, respectively, while the D−band–G−band ratio (I_D/I_G) reflects the LC defect degree of the carbon materials. The smaller the I_D/I_G, the higher the graphitization degree and crystallinity of the sample. The I_D/I_G ratios of N−ELC, N−ALC, and N−DLC were 1.21, 1.01, and 1.33, respectively. The I_D/I_G values of N−ALC were the lowest, and the graphitization degree was relatively high among several

lignins. The maximum I_D/I_G value of N−DLC indicates that there are more defects in this material [19].

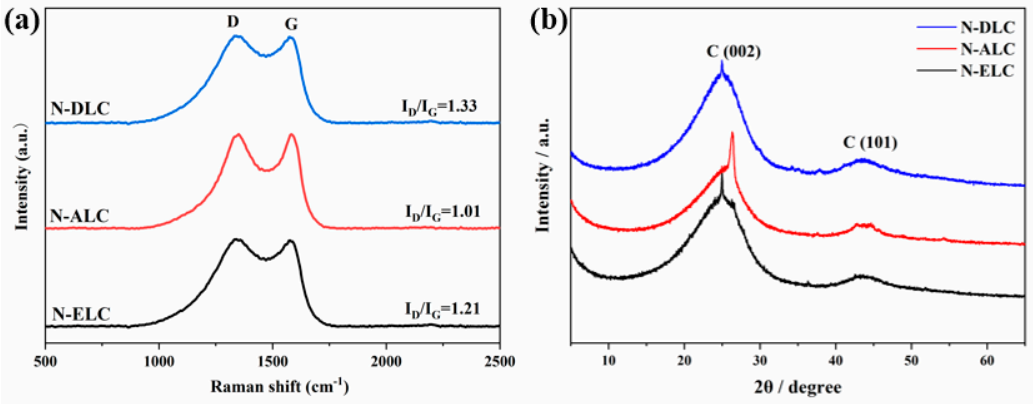

Figure 6. (**a**) Raman spectra and (**b**) XRD spectra of different kinds of lignin carbon materials.

At the same time, the crystal structures of different lignin carbon materials were characterized by XRD. The XRD patterns of N−ELC, N−ALC, and N−DLC showed two wide diffraction peaks (Figure 6b), whose centers were at approximately 25° and 43°, corresponding to the (002) and (101) crystal planes of graphitized carbon, respectively. Therefore, by using the strategy of melamine−assisted co−catalysis, the three lignin raw materials can produce relatively good graphite−structured carbon nanomaterials, which is consistent with the TEM results.

Specific surface area is a key factor affecting the oxygen reduction activity of carbon materials. A high specific surface area is conducive to exposing more oxygen reduction active sites, thereby improving the catalytic performance of the ORR [27]. Figure 7a shows the N_2 adsorption and desorption curves of different carbon materials. N−ELC, N−ALC, and N−DLC all show type−IV isotherm characteristics in the medium–high−pressure region (P/P_0 = 0.45~1), and there are obvious retention rings, indicating that there are abundant mesoporous structures. The pore size distribution was determined using the Barrett−Joyner−Halenda (BJH) equation, as shown in Figure 7b. The average pore size of the three carbon materials was mostly between 2~50 nm, among which N−ALC had an abundant mesoporous structure. The BET specific surface areas of N−ELC, N−ALC, and N−DLC were 55.82, 332.83, and 60.02 $m^2 \cdot g^{-1}$, respectively. The abundant mesoporous structure and large specific surface area of N−ALC may increase the exposed active sites and promote the mass diffusion and electron transfer of electrocatalysis, thereby achieving better electrocatalytic performance.

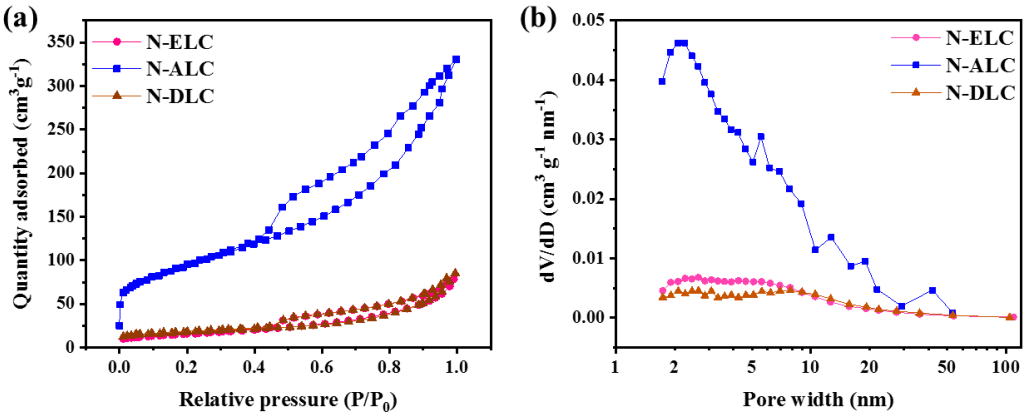

Figure 7. (**a**) N_2 adsorption–desorption isotherms of different lignin carbon materials. (**b**) Aperture distribution curve.

3.3. Electrocatalytic Oxygen Reduction Performance of Different Kinds of Lignin Carbon Materials

The ORR catalytic performance of lignin carbon materials was determined by cyclic voltammetry (CV). Cyclic voltammetry curves of the materials were measured in 0.1 M KOH solutions saturated with O_2 and N_2 (Figure 8a–c). It can be seen from the test results that the CV curves of the three different lignin–carbon catalysts in the N_2−saturated electrolyte do not show obvious redox peaks. In the O_2−saturated electrolyte, obvious reduction peaks appeared at approximately 0.82, 0.84, and 0.67 V, indicating that these carbon materials have electrocatalytic ORR activity.

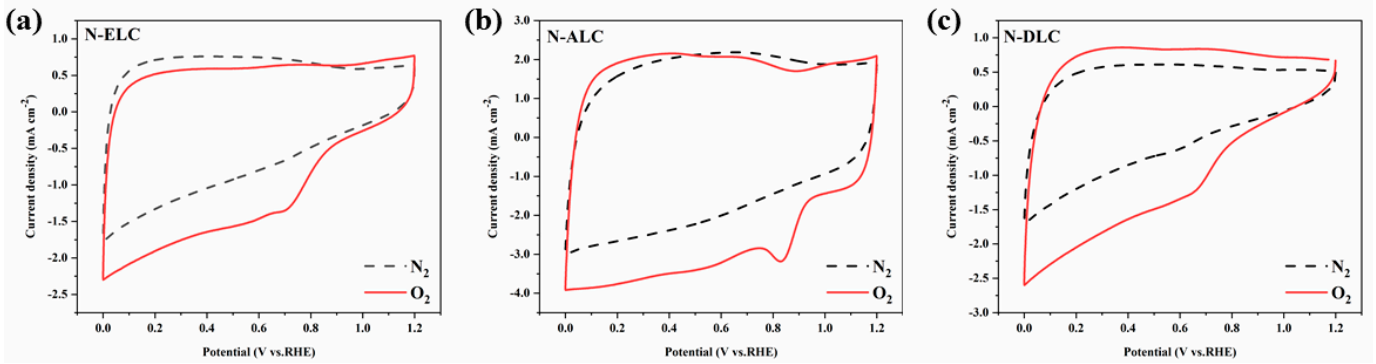

Figure 8. CV curves of different catalysts in O_2− and N_2−saturated electrolytes. (**a**) N−ELC; (**b**) N−ALC; (**c**) N−DLC.

Figure 9a shows the LSV curves of different lignin carbon materials at 1600 rpm, while Figure 9b shows a comparison of important visual indicators of electrocatalytic performance: half−wave potential ($E_{1/2}$), onset potential (E_{onset}), and limiting current density (j_d). As shown in Figure 9, N−DLC has the worst catalytic performance among the three lignins, while N−ALC and N−ELC both have good ORR performance. The $E_{1/2}$ and E_{onset} of N−ALC are 0.84 and 0.96 V, respectively, while the $E_{1/2}$ and E_{onset} of N−ELC are 0.82 and 0.93 V, respectively. Compared with the standard commercial performance of 20% Pt/C ($E_{1/2}$ = 0.86 V, E_{onset} = 0.98 V), the catalytic performance of N−ELC reached more than 95% of its catalytic performance. This indicated that compared with common alkaline lignin, although the specific surface area and pore volume of EL were smaller than those of AL, the ORR catalytic performance of EL was slightly lower than that of AL, but both had excellent catalytic performance. This indicates that EL could also be used as an excellent electrocatalyst raw material. The electrochemical performance parameters of biomass−based oxygen reduction electrocatalysts are listed in Table S1 (Supplementary Materials).

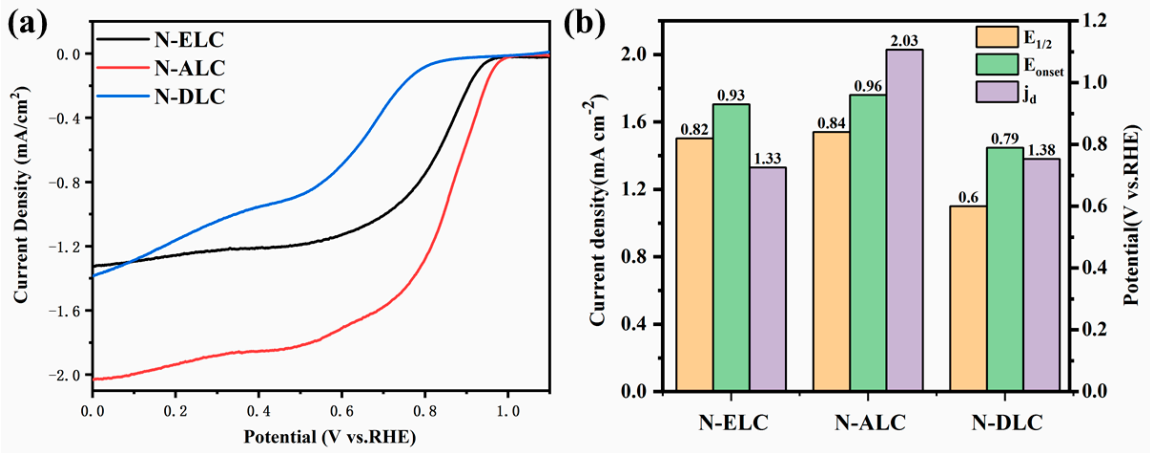

Figure 9. ORR performance: (**a**) LSV curve obtained at 1600 rpm. (**b**) Performance comparison bar chart.

4. Conclusions

In this paper, different lignin–nitrogen−doped porous carbon catalysts were prepared using EL, AL, and DL as carbon sources and melamine as the nitrogen source. The results show that, like AL, EL is also an excellent carbon source material for preparing electrocatalysts. The FTIR and UV−Vis results showed that the surface functional groups of the three kinds of lignin were similar. The thermal performance analysis showed that EL and AL had different pyrolysis processes, and that of AL was mainly a process of aryl ether bond breaking, methoxy group breaking, and side−chain dehydration forming small molecules. The electrocatalytic oxygen reduction results showed that N−ALC had the best ORR performance among the three materials. The $E_{1/2}$ and E_{onset} of N−ALC were 0.84 V and 0.96 V, respectively. The $E_{1/2}$ and E_{onset} of N−ELC were 0.82 and 0.93 V, respectively—slightly lower than those of N−ALC. Compared with the standard commercial performance of 20% Pt/C ($E_{1/2}$ = 0.86 V, E_{onset} = 0.98 V), the catalytic performance of N−ELC can reach more than 95% of its catalytic performance.

Supplementary Materials: The following supporting information can be downloaded at: https://www.mdpi.com/article/10.3390/ijerph20054383/s1, Table S1: Comparison of ORR performance of different lignin catalysts. References [28–31] are cited in the supplementary materials.

Author Contributions: Conceptualization, Z.L. and S.R.; Methodology, Z.L., S.R. and T.L.; Validation, Y.F.; Formal Analysis, Z.L. and X.Q.; Investigation, Y.F. and X.Q.; Resources, Y.Y. and S.R.; Data Curation, Z.L.; Writing—Original Draft, Z.L.; Writing—Review and Editing, S.R., Y.Y. and L.D.; Supervision, T.L. All authors have read and agreed to the published version of the manuscript.

Funding: This research was funded by the National Key Research and Development Program of China (grant number 2021YFC2101604).

Institutional Review Board Statement: Not applicable.

Informed Consent Statement: Not applicable.

Conflicts of Interest: The authors declare no conflict of interest.

References

1. Hussain, S.; Ullah, N.; Zhang, Y.; Shaheen, A.; Javed, M.S.; Lin, L.; Zulfiqar; Shah, S.B.; Liu, G.; Qiao, G. One−step synthesis of unique catalyst Ni9S8@C for excellent MOR performances. *Int. J. Hydrogen Energy* **2019**, *44*, 24525–24533. [CrossRef]
2. Samaniego, A.J.; Arabelo, A.K.; Sarker, M.; Mojica, F.; Madrid, J.; Chuang, P.-Y.A.; Ocon, J.; Espiritu, R. Fabrication of cellulose acetate−based radiation grafted anion exchange membranes for fuel cell application. *J. Appl. Polym. Sci.* **2021**, *138*, 49947. [CrossRef]
3. Ramasahayam, S.K.; Azam, S.; Viswanathan, T. Phosphorous, nitrogen co−doped carbon from spent coffee grounds for fuel cell applications. *J. Appl. Polym. Sci.* **2015**, *132*, 41948. [CrossRef]
4. Tao, H.; Gao, Y.; Talreja, N.; Guo, F.; Texter, J.; Yan, C.; Sun, Z. Two−dimensional nanosheets for electrocatalysis in energy generation and conversion. *J. Mater. Chem. A* **2017**, *5*, 7257–7284. [CrossRef]
5. Du, L.; Zhang, G.; Liu, X.; Hassanpour, A.; Dubois, M.; Tavares, A.C.; Sun, S. Biomass−derived nonprecious metal catalysts for oxygen reduction reaction: The demand−oriented engineering of active sites and structures. *Carbon Energy* **2020**, *2*, 561–581. [CrossRef]
6. Wang, G.; Wang, W.; Chen, Y.; Yan, C.; Gao, Z. Fe_3C decorated, N−doped porous carbon as cost−effective and efficient catalyst for oxygen reduction reaction. *Appl. Surf. Sci.* **2023**, *610*, 155456. [CrossRef]
7. Bouleau, L.; Perez−Rodriguez, S.; Quilez−Bermejo, J.; Izquierdo, M.T.; Xu, F.; Fierro, V.; Celzard, A. Best practices for ORR performance evaluation of metal−free porous carbon electrocatalysts. *Carbon* **2022**, *189*, 349–361. [CrossRef]
8. Liu, X.; Culhane, C.; Li, W.; Zou, S. Spinach−Derived Porous Carbon Nanosheets as High−Performance Catalysts for Oxygen Reduction Reaction. *ACS Omega* **2020**, *5*, 24367–24378. [CrossRef]
9. Sekhon, S.S.; Kaur, P.; Park, J.-S. From coconut shell biomass to oxygen reduction reaction catalyst: Tuning porosity and nitrogen doping. *Renew. Sustain. Energy Rev.* **2021**, *147*, 111173. [CrossRef]
10. Wang, C.; Kelley, S.S.; Venditti, R.A. Lignin−Based Thermoplastic Materials. *Chemsuschem* **2016**, *9*, 770–783. [CrossRef]
11. Huang, S.Q.; Su, S.Y.; Gan, H.B.; Wu, L.J.; Lin, C.H.; Xu, D.Y.; Zhou, H.F.; Lin, X.L.; Qin, Y.L. Facile fabrication and characterization of highly stretchable lignin−based hydroxyethyl cellulose self−healing hydrogel. *Carbohydr. Polym.* **2019**, *223*, 115080. [CrossRef]
12. Zhu, J.D.; Yan, C.Y.; Zhang, X.; Yang, C.; Jiang, M.J.; Zhang, X.W. A sustainable platform of lignin: From bioresources to materials and their applications in rechargeable batteries and supercapacitors. *Prog. Energy Combust. Sci.* **2020**, *76*, 100788. [CrossRef]

13. Kai, D.; Tan, M.J.; Chee, P.L.; Chua, Y.K.; Yap, Y.L.; Loh, X.J. Towards lignin−based functional materials in a sustainable world. *Green Chem.* **2016**, *18*, 1175–1200. [CrossRef]
14. Luis Espinoza−Acosta, J.; Torres−Chavez, P.I.; Olmedo−Martinez, J.L.; Vega−Rios, A.; Flores−Gallardo, S.; Armando Zaragoza−Contreras, E. Lignin in storage and renewable energy applications: A review. *J. Energy Chem.* **2018**, *27*, 1422–1438. [CrossRef]
15. Graglia, M.; Pampel, J.; Hantke, T.; Fellinger, T.-P.; Esposito, D. Nitro Lignin−Derived Nitrogen−Doped Carbon as an Efficient and Sustainable Electrocatalyst for Oxygen Reduction. *Acs Nano* **2016**, *10*, 4364–4371. [CrossRef] [PubMed]
16. Zhang, M.; Song, Y.; Tao, H.; Yan, C.; Masa, J.; Liu, Y.; Shi, X.; Liu, S.; Zhang, X.; Sun, Z. Lignosulfonate biomass derived N and S co−doped porous carbon for efficient oxygen reduction reaction. *Sustain. Energy Fuels* **2018**, *2*, 1820–1827. [CrossRef]
17. Li, P.; Wang, H.L.; Fan, W.J.; Huang, M.H.; Shi, J.; Shi, Z.C.; Liu, S. Salt assisted fabrication of lignin−derived Fe, N, P, S codoped porous carbon as trifunctional catalyst for Zn−air batteries and water−splitting devices. *Chem. Eng. J.* **2021**, *421*, 129704. [CrossRef]
18. Zhang, X.L.; Yu, D.L.; Zhang, Y.Q.; Guo, W.H.; Ma, X.X.; He, X.Q. Nitrogen− and sulfur−doped carbon nanoplatelets via thermal annealing of alkaline lignin with urea as efficient electrocatalysts for oxygen reduction reaction. *RSC Adv.* **2016**, *6*, 104183–104192. [CrossRef]
19. Shen, Y.; Li, Y.; Yang, G.; Zhang, Q.; Liang, H.; Peng, F. Lignin derived multi−doped (N, S, Cl) carbon materials as excellent electrocatalyst for oxygen reduction reaction in proton exchange membrane fuel cells. *J. Energy Chem.* **2020**, *44*, 106–114. [CrossRef]
20. Wang, Y.; Gan, R.; Zhao, S.; Ma, W.; Zhang, X.; Song, Y.; Ma, C.; Shi, J. B, N, F tri−doped lignin−derived carbon nanofibers as an efficient metal−free bifunctional electrocatalyst for ORR and OER in rechargeable liquid/solid−state Zn−air batteries. *Appl. Surf. Sci.* **2022**, *598*, 153891. [CrossRef]
21. Huang, B.; Jiang, J. N−doped carbon nanosheets derived from lignin as a novel bifunctional electrocatalyst for rechargeable zinc−air battery. *Diam. Relat. Mater.* **2022**, *128*, 109291. [CrossRef]
22. Wang, G.; Xia, Y.; Sui, W.; Si, C. Lignin as a Novel Tyrosinase Inhibitor: Effects of Sources and Isolation Processes. *ACS Sustain. Chem. Eng.* **2018**, *6*, 9510–9518. [CrossRef]
23. Ibarra, D.; del Rio, J.C.; Gutierrez, A.; Rodriguez, I.M.; Romero, J.; Martinez, M.J.; Martinez, A.T. Chemical characterization of residual lignins from eucalypt paper pulps. *J. Anal. Appl. Pyrolysis* **2005**, *74*, 116–122. [CrossRef]
24. Wang, X.; Guo, Y.; Zhou, J.; Sun, G. Structural changes of poplar wood lignin after supercritical pretreatment using carbon dioxide and ethanol−water as co−solvents. *RSC Adv.* **2017**, *7*, 8314–8322. [CrossRef]
25. Chen, X.; Wang, N.; Shen, K.; Xie, Y.; Tan, Y.; Li, Y. MOF−Derived Isolated Fe Atoms Implanted in N−Doped 3D Hierarchical Carbon as an Efficient ORR Electrocatalyst in Both Alkaline and Acidic Media. *ACS Appl. Mater. Interfaces* **2019**, *11*, 25976–25985. [CrossRef] [PubMed]
26. Lv, R.; Wang, H.; Yu, H.; Peng, F. Controllable Preparation of Holey Graphene and Electrocatalytic Performance for Oxygen Reduction Reaction. *Electrochim. Acta* **2017**, *228*, 203–213. [CrossRef]
27. Du, L.; Gao, X.Y.; Li, Z.; Yong, G.Y.; Wen, Z.; Yang, C.C.; Jiang, Q. Metal−organic frameworks derived Co/N−doped carbon nanonecklaces as high−efficient oxygen reduction reaction electrocatalysts. *Int. J. Hydrogen Energy* **2022**, *47*, 39133–39145. [CrossRef]
28. Shen, Y.; Peng, F.; Cao, Y.; Zuo, J.; Wang, H.; Yu, H. Preparation of nitrogen and sulfur co-doped ultrathin graphitic carbon via annealing bagasse lignin as potential electrocatalyst towards oxygen reduction reaction in alkaline and acid media. *J. Energy Chem.* **2019**, *34*, 33–42. [CrossRef]
29. Rois, M.F.; Widiyastuti, W.; Setyawan, H.; Rahmatika, A.M.; Ogi, T. Preparation of activated carbon from alkali lignin using novel one-step process for high electrochemical performance application. *Arab. J. Chem.* **2021**, *14*, 103162. [CrossRef]
30. Demir, M.; Farghaly, A.A.; Decuir, M.J.; Collinson, M.M.; Gupta, R.B. Supercapacitance and oxygen reduction characteristics of sulfur self-doped micro/mesoporous bio-carbon derived from lignin. *Mater. Chem. Phys.* **2018**, *216*, 508–516. [CrossRef]
31. Li, C.; Wu, Y.; Fu, M.; Zhao, X.; Zhai, S.; Yan, Y.; Zhang, L.; Zhang, X. Preparation of Fe/N Double Doped Carbon Nanotubes from Lignin in Pennisetum as Oxygen Reduction Reaction Electrocatalysts for Zinc-Air Batteries. *Acs Appl. Energy Mater.* **2022**, *5*, 4340–4350. [CrossRef]

Disclaimer/Publisher's Note: The statements, opinions and data contained in all publications are solely those of the individual author(s) and contributor(s) and not of MDPI and/or the editor(s). MDPI and/or the editor(s) disclaim responsibility for any injury to people or property resulting from any ideas, methods, instructions or products referred to in the content.